

# Influence of groove wheel discharger on the discharge pulsation characteristics of agricultural materials

Yu Ru<sup>1,2\*</sup>, Daming Xia<sup>1,3</sup>, Zifan Rong<sup>1</sup>, Xiao Zhang<sup>1</sup>

(1. College of Mechanical and Electronic Engineering, Nanjing Forestry University, Nanjing 210037, China;

2. Co-Innovation Center of Efficient Processing and Utilization of Forest Resources, Nanjing Forestry University, Nanjing 210037, China;

3. Wuxi Turbine Blade Co., Ltd, Wuxi, 214187, Jiangsu, China)

**Abstract:** The external groove wheel discharger has good versatility and can adapt well to materials of different particle sizes (seeds or fertilizers). However, the flow pulsation phenomenon during the working process may lead to a decrease in the efficiency of the operation, and thus optimization is needed. In this study, the straight-tooth groove wheel discharger was taken as the research object, and a discrete element model of the discharger in operation was established. The coefficient of variation of the flow pulsation was used as the evaluation index; the effective length of the groove wheel, the groove speed of the groove wheel, the arc length of the inverted tongue chamfer, and the radius of the concave groove were taken as the experimental factors; and a four-factor and five-level orthogonal regression rotation combination simulation experiment was conducted. A mathematical regression model of the coefficient of variation of the discharge pulsation was established to optimize each factor. The results showed that when the effective length of the groove wheel was 45 mm, the groove speed was 54 r/min, the arc length of the discharge tongue chamfer was 19 mm, and the groove radius was 12 mm, the coefficient of variation of the flow pulsation was optimal. The simulation results were consistent with the model predictions. Under the optimized parameters, simulation experiments on the flow pulsation of urea (spherical shape) and rice (ellipsoidal shape) particles were carried out separately. The results showed that under the same structure and working parameters, there were significant differences in the coefficient of variation of the flow pulsation between the two types of particles, with the rice particles having a larger overall coefficient of variation. Within the optimization constraint range of the groove speed, the coefficient of variation of the flow pulsation of rice particles gradually decreased and tended to be stable with the increase of the groove speed, while that of urea particles decreased first and then increased with the increase of the groove speed. After increasing the groove radius, the coefficient of variation of the flow pulsation of rice particles decreased overall, and the pulsation was improved, which was consistent with the results of the platform verification and simulation. Therefore, when using the external groove wheel discharger for different types of agricultural materials, the groove wheel can be replaced according to the different materials to meet the requirement of uniform discharge, which is conducive to the development of precision agriculture and of great significance.

**Keywords:** groove wheel, agricultural materials, discrete element method (DEM), response surface, optimal design

**DOI:** [10.25165/j.ijabe.20251801.8431](https://doi.org/10.25165/j.ijabe.20251801.8431)

**Citation:** Ru Y, Xia D M, Rong Z F, Zhang X. Influence of groove wheel discharger on the discharge pulsation characteristics of agricultural materials. *Int J Agric & Biol Eng*, 2025; 18(1): 83–91.

## 1 Introduction

Accurate control of seeding quantity is an important core content of precision agriculture<sup>[1,2]</sup>. Seeding quantity control mainly relies on the distributor, whose main function is to separate the material from the material box and control the discharge of the outlet. Its form and performance directly affect the quality of seeding operations. Due to the diverse types and physicochemical properties of agricultural materials, the distributor needs to have versatility and reduce usage costs. Among many types of

distributors, the groove wheel distributor has a small and simple structure, stable seeding quantity, and is easy to adjust. It has good adaptability to seeds of different particle sizes such as wheat and rice, and can also be used for the discharge of granular fertilizers and weeding agents, with good versatility<sup>[3,4]</sup>. However, during the operation of the groove wheel distributor, there is a flow pulsation phenomenon, and the material flow will cause breaks, resulting in discontinuous sedimentation areas and poor operational quality. Therefore, it is necessary to find an optimal structure and working parameters of the groove wheel to optimize the pulsation situation<sup>[5,6]</sup>.

The movement of materials in the groove wheel distributor is complex, involving various forces such as friction, squeezing, and collision. It is difficult to accurately analyze the movement of materials. However, the discrete element method can be effectively applied to solve this problem, and this method has been widely used in the field of agricultural engineering<sup>[7,8]</sup>.

To improve the uniformity of discharge, numerous scholars have conducted research on the parameter optimization of groove wheels<sup>[9-12]</sup>. Huang et al.<sup>[13]</sup> studied the influence of working parameters of the groove wheel on the pulsation of fertilizer particles during the discharge process, established a mathematical

**Received date:** 2023-07-18 **Accepted date:** 2024-11-05

**Biographies:** **Daming Xia**, MS, research interest: agriculture and forestry plant protection technology and equipment, Email: [xdmzq@njfu.edu.cn](mailto:xdmzq@njfu.edu.cn); **Zifan Rong**, PhD, research interest: agriculture and forestry plant protection technology and equipment, Email: [1054095896@qq.com](mailto:1054095896@qq.com); **Xiao Zhang**, MS research interest: agriculture and forestry plant protection technology and equipment, Email: [3266163556@qq.com](mailto:3266163556@qq.com).

**\*Corresponding author:** **Yu Ru**, PhD, Professor, research interest: agriculture and forestry plant protection technology and equipment. Nanjing Forestry University, Nanjing 210037, China. Tel: +86-13951778251, Email: [superchry@163.com](mailto:superchry@163.com).

regression model between them, and verified the feasibility of DEM simulation with consistent simulation and experimental results. Liu et al.<sup>[14]</sup> proposed a new particle counting method and developed a flow monitoring sensor to improve the accuracy of flow monitoring for wheat seeding in the groove wheel distributor, and the developed sensor can be applied in practice. Song et al.<sup>[15,16]</sup> designed groove wheels with different groove cross-sectional shapes and groove numbers and selected the fertilizer distributor that meets the requirements of drone fertilization. The research results showed that the cross-sectional shape and number of grooves have a significant impact on pulsation, and a fertilizer spreading rate control system with variable speed was designed accordingly. Su et al.<sup>[17]</sup> studied the influence of the adjustable working length of the groove wheel on variable rate fertilization. The average coefficient of variation under five different working lengths was 8.4%, reflecting good fertilization uniformity. Wang et al.<sup>[18]</sup> studied the influence of three factors - spiral angle, groove depth, and tooth ridge thickness of the groove wheel - on fertilization uniformity. The results showed that the distribution is most uniform when the spiral angle is 45°, the groove depth is 9 mm, and the tooth ridge thickness is 2 mm. Sugirbay et al.<sup>[19]</sup> designed a new groove (pin-roller) wheel structure and improved the uniformity of fertilizer discharge at low speeds by optimizing its structural parameters. Sun et al.<sup>[20]</sup> analyzed the velocity and force of particles during the operation of the groove wheel distributor using EDEM simulation software, manufactured it using 3D printing, and optimized the best working parameters of the groove wheel using response surface methodology. The relative error between EDEM simulation and the regression model and experiment was small.

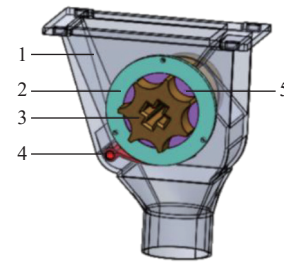
The above research provides important reference for the optimization of the groove wheel fertilizer distributor. However, current research on the groove wheel fertilizer distributor mainly focuses on the optimization of the working parameters or structural parameters of the groove wheel, and there is still a lack of research on the interaction between the two. On the other hand, when studying the flow pulsation of the groove wheel during operation, the research objects are mostly limited to a single type of fertilizer or seed. In practice, the groove wheel fertilizer distributor is used to regulate the dosage of various types of agricultural materials. Therefore, it is of great significance to conduct research on the flow pulsation of the groove wheel fertilizer distributor during the application process of different types of agricultural materials based on existing research. This paper takes the straight-tooth groove wheel fertilizer distributor as the research object, and uses discrete element simulation software to study the influence of single-factor and interactive effects on the flow pulsation of the discharge volume with the key working and structural parameters of the distributor as research factors. The optimal parameter combination of each factor is obtained, and the impact of the groove wheel fertilizer distributor on the flow pulsation of the discharge volume of different types of agricultural materials is studied under the optimized parameters.

## 2 Analysis of the working principles and structural parameters of groove wheel dischargers

### 2.1 Structural components of groove wheel dischargers

The groove wheel discharger mainly consists of a housing, a groove wheel, a discharge tongue, a blocking ring, etc., as shown in Figure 1. By rotating the groove wheel, the groove wheel discharger fills the material in the groove one by one and rotates it, and then

discharges it through the discharge tongue outlet, thereby transforming the discontinuous single particles into a continuous particle flow.



1. Shell 2. Flange ring 3. Groove wheel 4. Discharge tongue 5. Flower-shaped blocking ring

Figure 1 3D view of the outer groove wheel discharge device

### 2.2 Analysis of the key structural parameters of groove wheels

#### 2.2.1 Groove wheel

The key component of the groove wheel discharger is the groove wheel, which can adjust the discharge volume by changing the groove wheel rotation speed  $n$  and working length  $L$ . The index  $q$  ( $\text{cm}^3/\text{r}$ ), which means discharge volume per revolution, is the superposition of the forced layer and the driven layer, with the material driven by the teeth in the forced layer moving faster, while the material near the tooth ridges in the driven layer is pushed by friction at a slower speed.  $q$  can be calculated by Equation (1).

$$q = \pi d L \gamma \left( \frac{\alpha_0 f_q}{t} + \lambda \right) \quad (1)$$

where,  $d$  is the outer diameter of the groove wheel, cm;  $L$  is the effective working length of the groove wheel, cm;  $\gamma$  is the density of the material,  $\text{g}/\text{cm}^3$ ;  $\alpha_0$  is the material filling coefficient;  $f_q$  is the cross-sectional area of a single groove tooth,  $\text{cm}^2$ ;  $t$  is the pitch of the groove, cm;  $\lambda$  is the characteristic coefficient of the driven layer.

The effective length of the groove wheel is adjusted by the flower-shaped blocking ring. The blocking ring divides the groove wheel into an effective length and a non-effective length. The particles in the effective length can be discharged normally, while those in the non-effective length will accumulate and cannot be effectively discharged, as shown in Figure 2. The effective length of the groove wheel must satisfy Equation (2).

$$L_{\min} \geq (1.5 \sim 2.0) l \quad (2)$$

where,  $L_{\min}$  is the minimum working length of the groove wheel, mm;  $l$  is the average length of particles, mm.

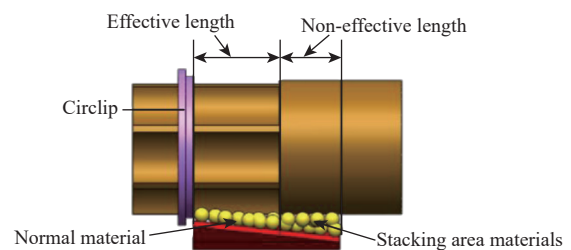


Figure 2 Effective length of groove wheel

The groove radius  $R$  affects the width  $b$  and depth  $h$  of the groove tooth. When the number of grooves remains constant, the larger the groove radius, the larger the width  $b$  and depth  $h$  of the groove tooth. The relative size of the tooth ridge between the groove teeth becomes smaller, and these parameters will affect the

stability of the discharge volume. The groove radius  $R$ , groove tooth width  $b$ , and depth  $h$  must satisfy Equation (3). The cross-section and ridge of the groove tooth are shown in Figure 3.

$$\begin{cases} 2R \geq 1 + b \\ 3b \leq h \leq l \end{cases} \quad (3)$$

where,  $R$  is the radius of the groove, mm;  $l$  is the average length of particles, mm;  $b$  is the width of the groove tooth, mm;  $h$  is the depth of the groove tooth, mm.

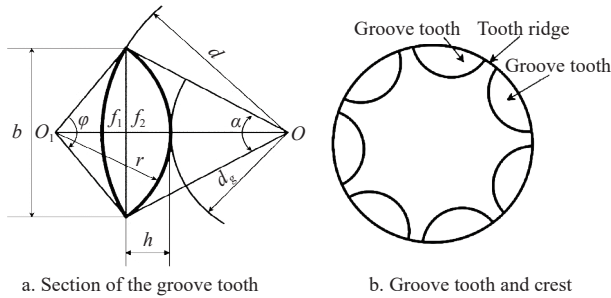


Figure 3 Section of the groove tooth and groove crest

2.2.2 Discharge tongue

Due to the tooth ridge on the groove wheel, the discharge volume is larger at the groove tooth position, forming a “peak”, while it is smaller at the tooth ridge position, forming a “valley”. The discharge volume will cyclically fluctuate between “peak” and “valley” with a certain periodicity, which affects the stability of the flow volume and is not conducive to precise control. To improve the stability of the flow volume, the outer end of the discharge tongue can be made into a tilted shape, so that the material flows continuously when the groove wheel moves to the discharge tongue outlet, as shown in Figure 4. The value of  $a$  is the arc length of the discharge tongue chamfer, which needs to be determined optimally, and the value of  $b$  is the width of the discharge tongue, which is related to the size of the discharger.

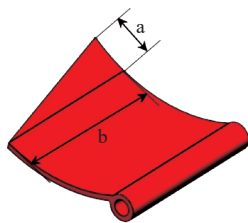


Figure 4 Arc length of the chamfer on the discharge tongue

Factors affecting the working performance of the discharger can be analyzed and divided into working parameters and structural parameters. Among the working parameters, the rotation speed and working length of the groove wheel have a greater impact, while among the structural parameters, the chamfer arc length of the discharge tongue and the groove radius have a greater impact.

The groove diameter is designed to be 55 mm, the number of grooves is 7, the maximum length of the groove is 60 mm, the discharge tongue width  $b$  is 60 mm and  $a$  is 0-30 mm, the groove speed is 30-70 r/min, and the groove radius is 10.5-12.5 mm.

3 Experimental materials and methods

According to the requirements of the EDEM software simulation calculation, it is necessary to establish a particle model and a discharger model, and to measure the three-axis size of the particles and determine the contact parameters between the two to conform to reality.

3.1 Determination and selection of agricultural particle parameters

Agricultural materials suitable for the groove wheel discharger can be divided into two categories based on their shapes. One is spherical particles, such as rapeseed, white cabbage seeds, granular fertilizers, etc. The other is ellipsoidal particles, such as rice, wheat, etc., as shown in Figure 5.

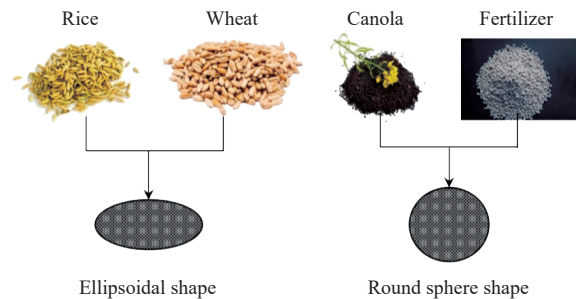


Figure 5 Classification of agricultural materials for groove wheel dischargers

This paper finally decided to study urea as the spherical particle and rice as the ellipsoidal particle. One hundred particles of each type were randomly selected, and their three-axis dimensions were measured using an electronic digital caliper (accuracy of 0.01 mm). The equivalent diameter and sphericity size of the two particles were calculated using Equations (4) and (5), respectively, as shown in Figure 6. The measurement results are listed in Table 1.

$$D = \sqrt[3]{LWT} \quad (4)$$

$$\phi = \frac{D}{L} \quad (5)$$

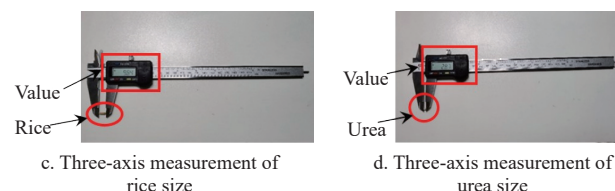
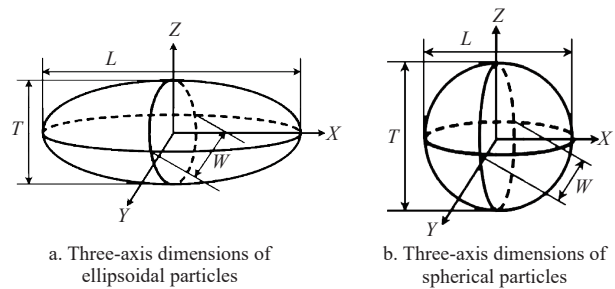


Figure 6 Two methods for measuring the three-axis dimensions of particles

Table 1 Important parameters for rice and urea

Particle type	Length/mm		Width/mm		Thickness/mm		Equivalent diameter/mm		Sphericity/mm	
	Mean	Standard deviation	Mean	Standard deviation	Mean	Standard deviation	Mean	Standard deviation	Mean	Standard deviation
Rice	9.31	0.508	2.18	0.089	1.92	0.053	3.39	0.085	36.46	0.016
Urea	2.31	0.309	2.21	0.365	2.27	0.260	2.26	0.311	97.97	0.024

where,  $D$  is the equivalent diameter of the particle, mm;  $L$  is the length dimension of the particle, mm;  $W$  is the width dimension of the particle, mm;  $T$  is the thickness dimension of the particle, mm;  $\phi$  is the sphericity of the particle, %.

According to the measurement results in Table 1, the average equivalent diameter and sphericity of rice particles are 3.39 mm and 36.46%, respectively, while those of urea particles are 2.26 mm and 97.97%, respectively. The results show that the difference in shape between the two particles is significant, and urea is selected as the spherical particle while rice is selected as the ellipsoidal particle, which meets the expected selection requirements.

### 3.2 Determination of contact model and parameters

EDEM software provides multiple contact models. Considering that the study in this paper does not involve the adhesion effect between particles, the Hertz-Mindlin (no sliding) contact model is used for the contact between particles and between particles and each part of the discharger<sup>[21,22]</sup>. The materials of each part of the outer trough discharger are all ABS. The contact parameters between particle-particle and particle-geometry model are determined by a combination of experimental measurement and literature review<sup>[23-25]</sup>, as listed in Table 2.

**Table 2 Discrete element simulation parameters**

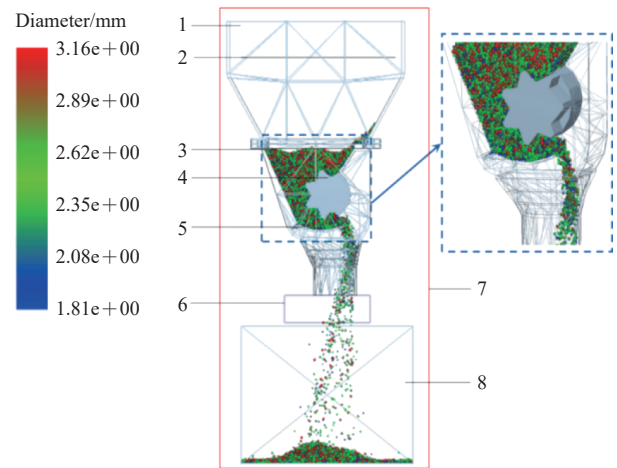
Material	Parameter	Value		
ABS	Poisson ratio	0.394		
	Density/(kg·m <sup>-3</sup> )	1060		
	Shear modulus	8.9×10 <sup>8</sup>		
Urea	Poisson ratio	0.250		
	Density/(kg·m <sup>-3</sup> )	1330		
	Shear modulus	3.48×10 <sup>7</sup>		
Rice	Poisson ratio	0.300		
	Density/(kg·m <sup>-3</sup> )	1077		
	Shear modulus	1.08×10 <sup>8</sup>		
Urea-Urea	Rice-Rice	Coefficient of restitution	0.35	0.42
	Urea-ABS	Rice-ABS	Static friction coefficient	0.30
Rice-Rice		Rolling friction coefficient	0.26	0.01
		Rice-ABS	Coefficient of restitution	0.60
Static friction coefficient	0.17		0.58	
Rolling friction coefficient	0.01		0.01	

### 3.3 Construction of discrete element simulation model

#### 3.3.1 Groove wheel discharger and particles simulation model

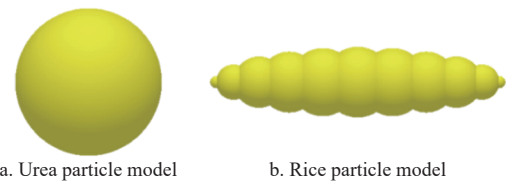
To improve the efficiency of simulation calculation, the discharger simulation test model was simplified by retaining only key components. The discharge outlet of the groove wheel discharger was equipped with a discharge pulsation monitoring area (100 mm×100 mm×30 mm), and a collection box (200 mm×150 mm×150 mm) was placed at the bottom to collect the falling materials. To approximate the real situation, the particle factory adopts the dynamic generation method to generate 30 000 particles within 1s, with a falling speed of 1 m/s and a gravity acceleration of 9.81 m/s<sup>2</sup>. The Rayleigh time step length is 25%. When the particle generation is completed and stabilized, the groove wheel starts to rotate, as shown in Figure 7.

Based on the three-axis measurements in Table 1, a spherical model can be used to approximate the urea particles in the simulation, while 11 spherical models can be overlaid to form the rice particles, as shown in Figure 8. The diameter of the urea model is 2.26 mm, and the length, width, and height of the rice particles are 9.3 mm×2.2 mm×2.2 mm. The equivalent diameters of both particles follow a normal distribution pattern, set according to Table 1.



1. Material box 2. Particle factory 3. Discharge box 4. Trough wheel 5. Discharging tongue 6. Flow fluctuation monitoring area 7. Simulation calculation domain 8. Collection box

Figure 7 EDEM simulation test model of the discharger



a. Urea particle model b. Rice particle model

Figure 8 Discrete element simulation model of particles

#### 3.3.2 Evaluation index

The coefficient of variation can measure the dispersion of sample data, and the flow pulsation refers to the fluctuation of the mass of particle flow in the flow pulsation monitoring area within the same time interval. The smaller the variation coefficient of flow pulsation, the smaller the mass fluctuation of particle flow, and the more stable the flow.

The urea particle model is simple, and the simulation efficiency is high. In order to obtain the variation law of the groove wheel discharger under different parameters, urea particles are used as the test object for simulation. The total simulation time is 5 s, and the data is saved every 0.05 s. The stable working stage of the discharger is captured for data analysis, which is between 2-4 s. The mass of the particle flow passing through the flow pulsation monitoring area is recorded every 0.1 s. The coefficient of variation of the flow pulsation is used as the evaluation index, calculated as shown in Equation (6).

$$\bar{m} = \frac{\sum_{i=1}^n m_i}{n}, s = \sqrt{\frac{\sum_{i=1}^n (m_i - \bar{m})^2}{n-1}}, C_V = \frac{s}{\bar{m}} \times 100\% \quad (6)$$

where,  $m$  is the average value of all data in the flow pulsation monitoring area, g;  $m_i$  is the mass of a specific data point collected in the flow pulsation monitoring area, g;  $s$  is the standard deviation of all data samples in the flow pulsation monitoring area;  $i$  is the number of data points collected in the flow pulsation monitoring area;  $n$  is the total number of data points collected in the flow pulsation monitoring area;  $C_V$  is the coefficient of variation of flow pulsation, %.

#### 3.3.3 Factor encoding and experimental design

This study adopts a four-factor five-level orthogonal regression rotation combination experimental design<sup>[13,20]</sup>. Factor  $A$  represents the effective length of the groove, factor  $B$  represents the groove

speed, factor *C* represents the arc length of the discharge tongue chamfer, and factor *D* represents the groove radius. The experimental factor coding is presented in Table 3, a response surface central composite design was conducted, and the experimental design and results are listed in Table 4.

**Table 3 Factor coding and experimental level table**

Encoding	Factor			
	<i>A</i> /mm	<i>B</i> /r·min <sup>-1</sup>	<i>C</i> /mm	<i>D</i> /mm
-2	20	30	0.0	10.5
-1	30	40	7.5	11.0
0	40	50	15.0	11.5
1	50	60	22.5	12.0
2	60	70	30.0	12.5

**Table 4 Results of response surface central composite experiment design**

Experiment	Factor				Results <i>C<sub>V</sub></i> %
	<i>A</i> /mm	<i>B</i> /r·min <sup>-1</sup>	<i>C</i> /mm	<i>D</i> /mm	
1	-1	-1	-1	-1	10.5724
2	1	-1	-1	-1	11.6366
3	-1	1	-1	-1	10.8777
4	1	1	-1	-1	9.8368
5	-1	-1	1	-1	13.6206
6	1	-1	1	-1	11.0602
7	-1	1	1	-1	12.4436
8	1	1	1	-1	8.0859
9	-1	-1	-1	1	9.8149
10	1	-1	-1	1	10.7639
11	-1	1	-1	1	10.2240
12	1	1	-1	1	9.9405
13	-1	-1	1	1	11.0154
14	1	-1	1	1	8.6526
15	-1	1	1	1	8.5712
16	1	1	1	1	6.2821
17	-2	0	0	0	13.0814
18	2	0	0	0	8.2070
19	0	-2	0	0	12.1867
20	0	2	0	0	10.6413
21	0	0	-2	0	9.5928
22	0	0	2	0	9.7099
23	0	0	0	-2	8.3065
24	0	0	0	2	6.6887
25	0	0	0	0	8.8419
26	0	0	0	0	7.9469
27	0	0	0	0	7.7398
28	0	0	0	0	7.5170
29	0	0	0	0	7.5165
30	0	0	0	0	8.4973

**4 Results and discussion**

**4.1 Regression analysis**

Based on the experimental results presented in Table 4, the Design-expert 11 software was used to perform multivariate regression fitting analysis of the experimental data. The results of the regression model variance analysis are listed in Table 5. The evaluation index of the variance analysis is represented by the *p* value, where a smaller *p* value indicates a more reliable regression model. Specifically, *p*<0.01 indicates extremely significant, *p*<0.05 indicates significant, and other values are not significant. The

results show that the quadratic regression model (*p*<0.0001) is extremely significant, and the lack-of-fit term (*p*=0.2799) is not significant. The model's coefficient of determination, *R*<sup>2</sup>=0.9335, and *R*<sub>adj</sub><sup>2</sup>=0.8715 are close to 1 and the difference between them is small, indicating a good fit between the regression model and the simulation experiment results. Significant analysis was performed on each single factor, and the order of the main and secondary factors affecting the variation coefficient of discharge pulsation from largest to smallest was *A* (extremely significant), *B* (extremely significant), *D* (extremely significant), and *C* (not significant). Among the interaction terms of the four factors, only *AC*, *BC*, and *CD* have an impact on the variation coefficient of discharge pulsation, and the order of their influence from largest to smallest is *AC* (extremely significant), *CD* (extremely significant), and *BC* (significant). After eliminating the insignificant factors in the regression model, the regression equation for *C<sub>V</sub>* is obtained as shown in Equation (7).

$$C_V = 8.01 - 0.86A - 0.58B - 0.67D - 0.77AC - 0.44BC - 0.53CD + 0.73A^2 + 0.92B^2 + 0.48C^2 \quad (7)$$

**Table 5 Analysis of variance results**

Source	<i>df</i>	Mean square	<i>F</i> -value	<i>p</i> -value	Significant
Model	14	6.7300	15.0500	<0.0001	**
<i>A</i>	1	17.7300	39.6700	<0.0001	**
<i>B</i>	1	8.1300	18.1800	0.0007	**
<i>C</i>	1	0.5707	1.2800	0.2762	-
<i>D</i>	1	10.8100	24.1800	0.0002	**
<i>AB</i>	1	1.6000	3.5800	0.0779	-
<i>AC</i>	1	9.3900	21.0100	0.0004	**
<i>AD</i>	1	0.5287	1.1800	0.2940	-
<i>BC</i>	1	3.1100	6.9600	0.0186	*
<i>BD</i>	1	0.0109	0.0243	0.8782	-
<i>CD</i>	1	4.5200	10.1200	0.0062	**
<i>A</i> <sup>2</sup>	1	14.5000	32.4300	<0.0001	**
<i>B</i> <sup>2</sup>	1	23.1900	51.8700	<0.0001	**
<i>C</i> <sup>2</sup>	1	6.2900	14.0700	0.0019	**
<i>D</i> <sup>2</sup>	1	0.0976	0.2183	0.6471	-
Residual	15	0.4470	-	-	-
Lack of Fit	10	0.5212	1.7500	0.2799	-
Pure Error	5	0.2986	-	-	-
Cor Total	29	-	-	-	-

Note: \* Significant \*\*Extremely significant

**4.2 Response surface analysis**

According to the variance analysis results in Table 5, only *AC*, *BC*, and *CD* have an effect on the variation coefficient of flow pulsation among the interaction terms of each factor, and response surface analysis needs to be performed on these three interaction terms.

**4.2.1 AC interaction response surface**

With *B*=50 r/min and *D*=11.5 mm, the interaction response surface of the effective length of the groove and the arc length of the discharge tongue chamfer is shown in Figure 9a, and the contour plot is shown in Figure 9b. In the non-abnormal area, when the effective length of the groove is kept constant, the variation coefficient of flow pulsation decreases first and then increases with the increase of the arc length of the discharge tongue chamfer; when the arc length of the discharge tongue chamfer is kept constant, the variation coefficient of flow pulsation first decreases and then increases with the increase of the effective length of the groove.

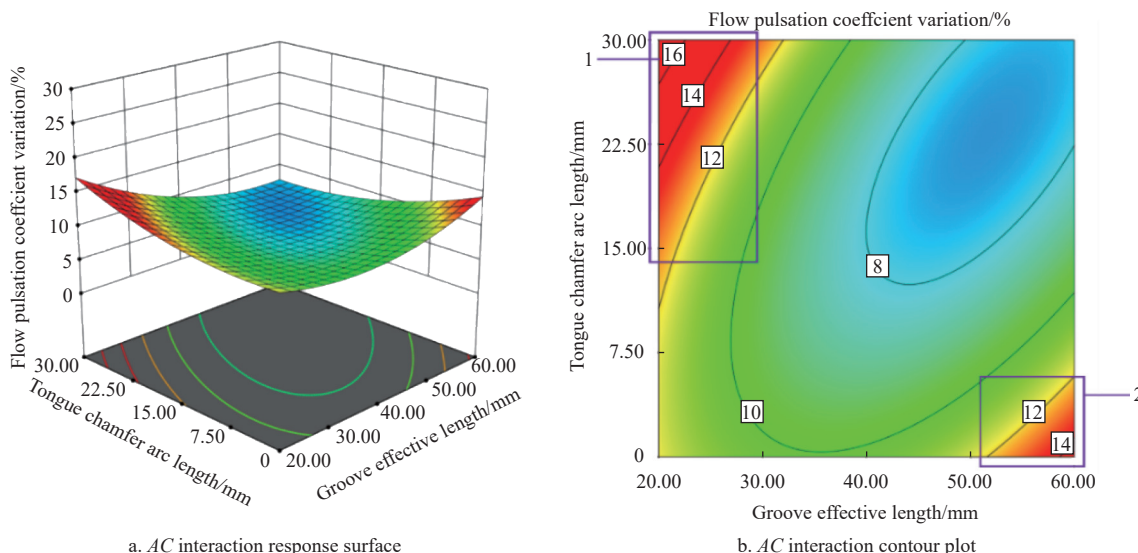


Figure 9 Influence of AC interaction on pulsation coefficient

In the abnormal area, when the effective length of the groove tends to be 20-30 mm and the arc length of the discharge tongue chamfer is 15-30 mm (Region 1), and when the effective length of the groove is 50-60 mm and the arc length of the discharge tongue chamfer is 0-5 mm (Region 2), the variation coefficient of flow pulsation is generally larger. The reasons for this are: (1) In Region 1, the effective length of the groove is short, and the accumulation of particles in the non-working section affects the entire discharge process, resulting in an increase in the variation coefficient of flow pulsation; (2) In Region 2, the arc length of the discharge tongue chamfer is small, and the increase of the effective length of the groove will cause some particles to overflow from the discharge tongue end with the rotation of the groove, thus affecting the variation coefficient of flow pulsation.

4.2.2 BC interaction response surface

With  $A=40$  mm and  $D=11.5$  mm, the interaction response surface of the groove speed and the arc length of the discharge tongue chamfer is shown in Figure 10a, and the contour plot is shown in Figure 10b. In the non-abnormal region, when the groove speed is kept constant, the coefficient of variation of the flow first decreases and then increases with the increase of the arc length of the discharge tongue chamfer. When the arc length of the discharge tongue chamfer is kept constant, the coefficient of variation of the flow first

decreases and then increases with the increase of the groove speed.

In the abnormal region, when the groove speed tends to be 30-35 r/min and the arc length of the discharge tongue chamfer is 0-30 mm (Region 1), or when the arc length of the discharge tongue chamfer is 0-7.5 mm and the groove speed is 60-70 r/min (Region 2), the variation coefficient of flow pulsation is generally larger. The reasons for this are: (1) In Region 1, the groove speed is low, and the overall flow rate of the forced layer and the driven layer particles decreases, affecting the coefficient of variation of the flow. When the arc length of the discharge tongue gradually increases, the flow pulsation is improved to some extent, but when it continues to increase, the arc length of the discharge tongue becomes too long, and some particles will flow out naturally from the other end of the corner gap, leading to an increase in the coefficient of variation of the flow; (2) In Region 2, when the groove speed is fast and the arc length of the discharge tongue chamfer is small, more particles flow out from the discharge tongue chamfer end in the driven layer, which weakens the effect of the discharge tongue chamfer design and affects the coefficient of variation of the flow pulsation.

4.2.3 CD interaction response surface

With  $A=40$  mm and  $B=50$  r/min, the response surface of the arc length of the discharge tongue chamfer and the groove radius is shown in Figure 11a, and the contour plot is shown in Figure 11b.

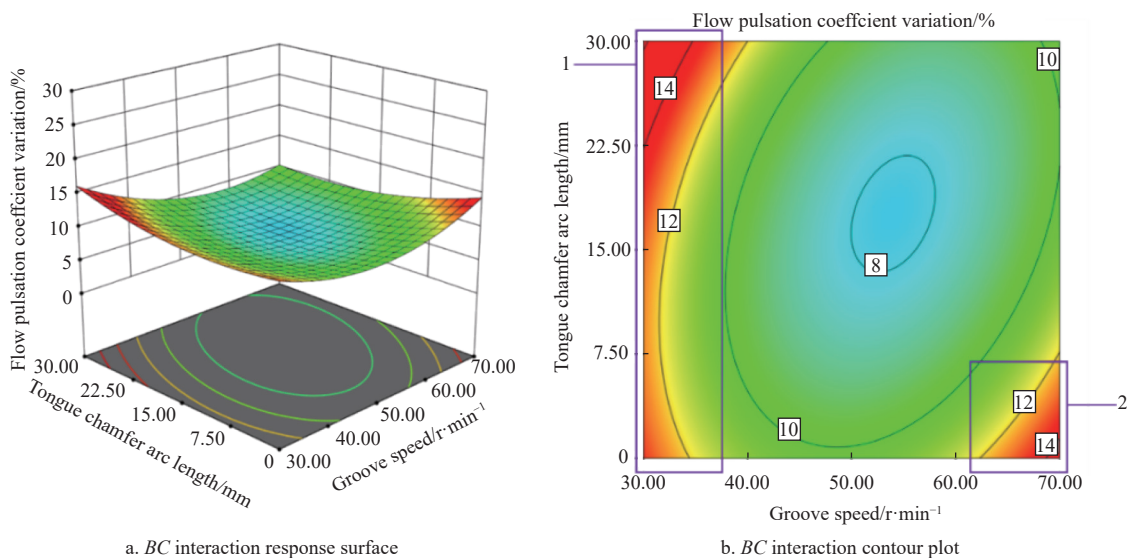


Figure 10 Influence of BC interaction on pulsation coefficient

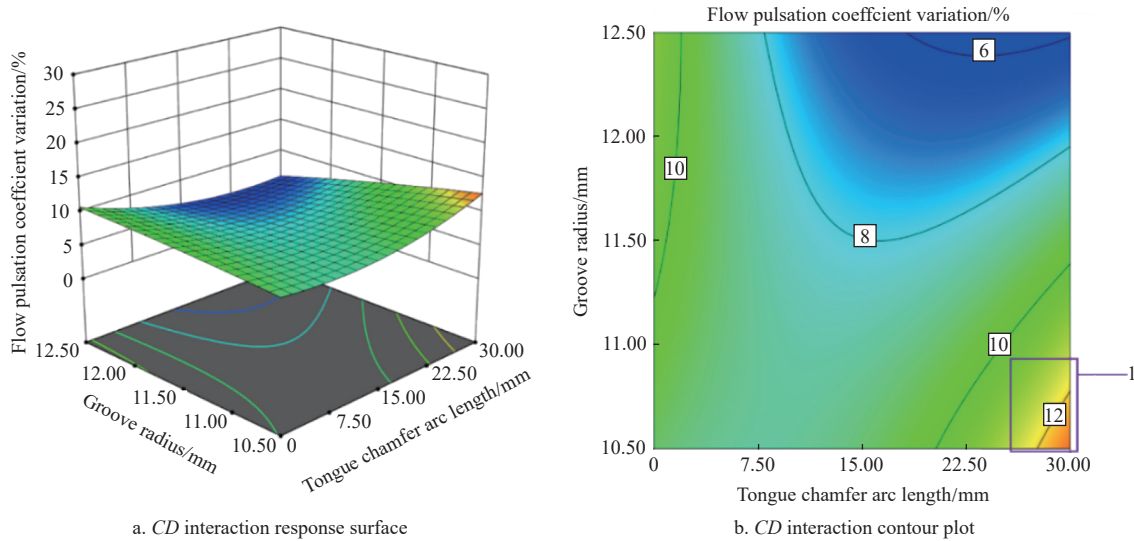


Figure 11 Influence of CD interaction on pulsation coefficient

In the non-abnormal region, when the groove radius is kept constant, the coefficient of variation of the flow decreases first and then increases with the increase of the arc length of the discharge tongue chamfer. When the arc length of the discharge tongue chamfer is kept constant, the coefficient of variation of the flow pulsation gradually decreases with the increase of the groove radius. In the abnormal region, when the arc length of the discharge tongue chamfer tends to 30 mm and the groove radius tends to 10.5 mm (Region 1), the coefficient of variation of the flow pulsation is generally larger.

The reason for this is: In Region 1, the groove radius is small, and the teeth ridges between the grooves increase, resulting in a longer discharge time interval for the forced layer particles to flow out. Moreover, when the arc length of the discharge tongue chamfer is too large, the particles will also flow out from the other end of the chamfer, affecting the coefficient of variation of the flow pulsation.

**4.3 Experimental results and target optimization**

In order to reduce the flow pulsation during the discharging process and find an optimal combination of structural and operational parameters for the discharger to achieve better performance, the evaluation index of coefficient of variation of discharge pulsation was taken as the objective function, while the factors listed in Table 3 were used as constraint conditions and the boundary conditions were defined by Equation (8). The goal was to obtain the minimum value of the coefficient of variation of discharge pulsation.

$$\begin{cases} \min C_v(A, B, C, D) \\ \text{s.t.} \begin{cases} 30 \text{ mm} \leq A \leq 60 \text{ mm} \\ 40 \text{ r/min} \leq B \leq 70 \text{ r/min} \\ 7.5 \text{ mm} \leq C \leq 22.5 \text{ mm} \\ 11 \text{ mm} \leq D \leq 12.5 \text{ mm} \end{cases} \end{cases} \quad (8)$$

Based on the multi-objective optimization solution above, the optimized parameter combination is listed in Table 6. The predicted values of the model under the optimization conditions have small errors compared with the actual simulation values, indicating that the established model is reliable and can be used for prediction.

Due to the different demands for agricultural materials handling, the required flow rate varies. Therefore, in addition to ensuring stability during operation, the groove wheel discharger must also be able to adjust the flow rate to meet the requirements of

different operations. In practice, it is more convenient to adjust the working parameters of the groove wheel than the structural parameters, as no replacement of parts is required. Moreover, according to the analysis of variance in Table 5, the effective length of the groove wheel has a greater effect on the coefficient of variation of flow rate pulsation than the rotational speed of the groove wheel. The flow rate can be adjusted according to the motor speed, with a wider range of adjustment, making it more convenient. Therefore, the flow rate can be controlled by changing the rotational speed of the groove wheel.

**Table 6 Comparison of predicted values and actual values under optimized conditions**

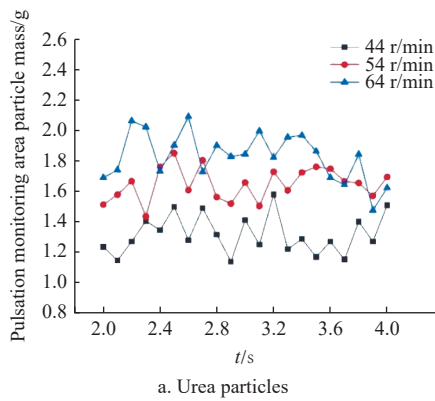
	Groove effective length/mm	Groove speed/r·min <sup>-1</sup>	Tongue chamfer arc length/mm	Groove radius/mm	Flow pulsation coefficient/%
Best conditions (Predicted value)	45.085	54.176	18.315	12.180	6.1812
Modified conditions (Actual value)	45.000	54.000	19.000	12.000	6.6169

Under the modified conditions of the optimized parameters in Table 6, while keeping the other optimized parameters constant, simulations were performed on rice and urea particles using the groove wheel at different rotational speeds. The change in mass of particles passing through the flow rate pulsation monitoring area with time is shown in Figure 12.

According to the analysis of Figure 12, with the increase of the speed of the groove wheel, the mass of particles passing through the monitoring area of flow fluctuation per unit time increases, and the discharge increases with the increase of the groove speed. Among them, the mass fluctuation of urea particles under different groove wheel speeds is small, and the fluctuation in the discharge process is better, while the mass fluctuation of rice particle flow under different groove wheel speeds is large, the flow pulsation in the discharge process is large, and the discharge stability is poor.

The discharge pulsation coefficient of the two types of particles under different groove wheel speeds is listed in Table 7. It can be seen that under the same parameter conditions, there is a significant difference in the flow pulsation coefficient between rice and urea particles, and the overall discharge pulsation coefficient of rice particles is larger, especially at low speeds. With the increase of the groove speed, the pulsation situation improves. Within the optimized range of groove speed constraints, the flow pulsation coefficient of

urea particles decreases first and then increases with the increase of speed, which is consistent with the prediction of the regression



model. The flow pulsation coefficient of rice particles decreases gradually with the increase of speed and tends to be stable.

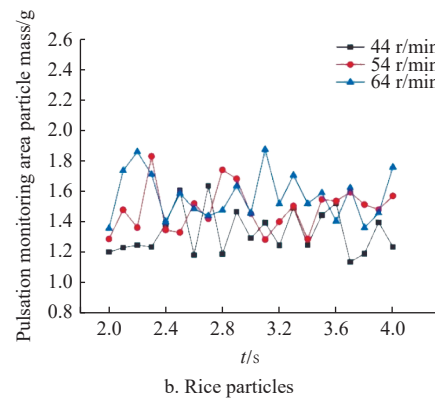


Figure 12 Variation of mass flow passing through the pulsation monitoring area over time for two particles

Table 7 Variation coefficient of flow pulsation of two kinds of particles

Particle type	Flow pulsation coefficient variation		
	44 r·min <sup>-1</sup>	54 r·min <sup>-1</sup>	64 r·min <sup>-1</sup>
Urea	9.7409	6.6169	8.6569
Rice	27.8072	21.6383	20.4147

According to the analysis of variance in Table 5, besides working parameters, the factor that has the greatest influence on the variation coefficient of flow pulsation among the main factors is the groove radius in the structural parameters. In order to optimize the pulsation of rice particle discharge, with all other parameters being constant, the groove radius was increased to 12.5 mm. The simulation results of the variation coefficient of flow pulsation for rice particles before and after optimization are compared in Table 8.

54 r/min, and 64 r/min, respectively, flow tests were carried out for both rice and urea particles. The particles falling from the discharger within 1 s were collected and weighed, and the flow capacity of the two types of particles was calculated and converted. Each test was repeated five times, and the coefficient of variation of the flow capacity of the two types of particles under repeated tests was calculated using Equation (6). The experimental results are listed in Table 9.

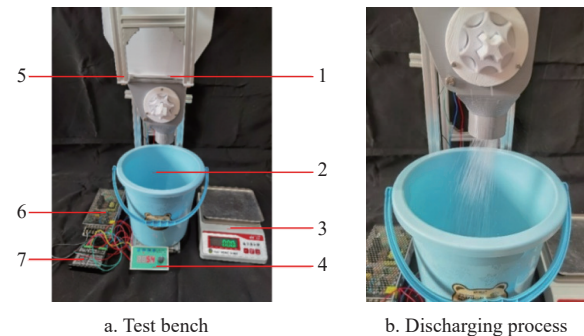
Table 8 Variations of flow pulsation coefficient for rice particles before and after optimization

Rice	Flow pulsation coefficient variation		
	44 r·min <sup>-1</sup>	54 r·min <sup>-1</sup>	64 r·min <sup>-1</sup>
Before optimization	27.8072	21.6383	20.4147
After optimization	25.5214	18.8426	18.0115

From Table 8, it can be seen that the pulsatility of rice grain displacement is improved after increasing the groove radius. Therefore, in the actual application process, when using a groove wheel discharger to discharge materials with large differences in shape and size, for some elliptical-shaped and larger-sized particles, the pulsatility during operation can be reduced by replacing the groove with a larger groove radius and appropriately increasing the groove speed within a suitable range, to meet the requirements of stable flow capacity for different materials.

#### 4.4 Discharger performance test

To further verify the reliability of the quadratic regression model established in the previous section and the EDEM simulation test results, a verification test was conducted using a 3D printed discharger and a self-made frame, where the 3D printed material was consistent with the simulation test material, as shown in Figure 13. Rice and urea particles were used under the same conditions as in the simulation test, and the other optimized parameters were kept constant. Since it is not possible to capture the mass flow rate of the selected particle flow every 0.1 s as in the simulation, the experimental verification scheme proposed in this paper is as follows: except for the groove speed, other optimized parameters are kept constant, and at groove speeds of 44 r/min,



a. Test bench b. Discharging process

1. Discharger
2. Bracket
3. Collection area
4. 24V switch power supply
5. 42 stepper motor
6. Driver
7. Programmable controller

Figure 13 Discharge verification test

Table 9 Comparison of performance tests and simulations for two types of particles

Particle type	Groove Speed/r·min <sup>-1</sup>	Flow/g·s <sup>-1</sup>		Flow pulsation coefficient variation/%
		Simulated value	Test value	Value
Urea	44	54.18	54.07	2.39
	54	66.95	65.38	2.24
	64	75.18	73.55	2.63
Rice	44	23.49	22.88	2.58
	54	28.80	28.66	2.43
	64	33.77	35.51	2.59

From the results in Table 9, it can be seen that there is a certain deviation in the displacement between the simulation results and the bench test results for both types of particles. This is mainly because there is a certain deviation in the control motor startup and shutdown and actual speed. Additionally, the sizes of the two types of particles are not strictly normally distributed and have some “flaws”. However, the error between the measured values and the simulation is small, and the coefficient of variation of the displacement obtained in repeated experiments is less than 5%. The mass fluctuation of the discharge in multiple tests of the discharger is also small. Therefore, it can be considered that the simulation

results and the measured results are basically consistent, and the regression model established above is reliable.

## 5 Conclusions

1) A groove wheel discharger was designed with the displacement pulsation coefficient as the evaluation index. Orthogonal regression rotation combination simulation was used to study the effects of the effective length of the groove, groove speed, arc length of the discharge tongue chamfer, and groove radius on the displacement pulsation. The results show that the order of the single-factor impact on the pulsation is as follows, from largest to smallest: groove speed (extremely significant), effective length of the groove (extremely significant), groove radius (significant), arc length of the discharge tongue chamfer (not significant). Among the interaction terms, the impact of the effective length of the groove and the arc length of the discharge tongue chamfer on the displacement pulsation coefficient is the largest (extremely significant), followed by the arc length of the discharge tongue chamfer and the groove radius (extremely significant), and the groove speed and arc length of the discharge tongue chamfer (significant), while the others are not significant.

2) A regression mathematical model for the displacement pulsation coefficient was established and optimized to obtain the best combination parameters: groove effective length of 45.085 mm (rounded to 45 mm), groove speed of 54.176 r/min (rounded to 54 r/min), arc length of the discharge tongue chamfer of 18.315 mm (rounded to 19 mm), and groove radius of 12.180 mm (rounded to 12 mm). Under these optimized conditions, the predicted flow pulsation coefficient of the model was 6.1812%, and the actual simulated result of the flow pulsation coefficient under modified conditions was 6.6169%, which is basically consistent with the model prediction.

3) Under the optimized parameter combination, the pulsation of the flow for two types of particles, namely spherical (urea) and ellipsoidal (rice), was studied. The results show that there is a significant difference in the flow pulsation coefficient between the two types of particles under the same parameters. Within the optimized range of groove speed, the flow pulsation coefficient of rice particles decreases gradually as the speed increases and tends to be stable, while the flow pulsation coefficient of urea particles first decreases and then increases with increasing speed. After increasing the groove radius, the flow pulsation of rice particles is improved. The bench test results are basically consistent with the simulation results. Therefore, in practical applications, the groove wheel discharger can meet the requirements of uniform discharge for different types of agricultural materials by replacing the groove wheel.

## Acknowledgements

This project has received funding from the National Key Research and Development Plan of China (Grant No. 2018YFD0600202-04). The authors would like to thank Fengbo Yang, Nanjing Forestry University, for linguistic assistance during the preparation of this manuscript.

## [References]

- Zhang W F, Cao G X, Li X L, Zhang H Y, Wang C, Liu Q Q, et al. Closing yield gaps in China by empowering smallholder farmers. *Nature*, 2016; 537: 671–674.
- Zhu Q X, Wu G P, Chen L P, Zhao C J, Meng Z J. Influences of structure parameters of straight flute wheel on fertilizing performance of fertilizer apparatus. *Transactions of the CSAE*, 2018; 34(18): 12–20. (in Chinese)
- Xi X B, Gu C J, Shi Y J, Zhao Y, Zhang Y F, Zhang Q, et al. Design and experiment of no-tube seeder for wheat sowing. *Soil & Tillage Research*, 2020; 204: 104724.
- Song C C, Zhou Z Y, Luo X W, Lan Y B, He X G, Ming R, et al. Design and test of centrifugal disc type sowing device for unmanned helicopter. *Int J Agric & Biol Eng*, 2018; 11(2): 55–61.
- Zeng S, Tan Y P, Wang Y, Luo X W, Yao L M, Huang D P, et al. Structural design and parameter determination for fluted-roller fertilizer applicator. *Int J Agric & Biol Eng*, 2020; 13(2): 101–110.
- Shi Y Y, Chen M, Wang X C, Odhiambo M O, Zhang Y N, Ding W M. Analysis and experiment of fertilizing performance for precision fertilizer applicator in rice and wheat fields. *Transactions of the CSAM*, 2017; 48(7): 97–103.
- Coetzee J C. Calibration of the discrete element method and the effect of particle shape. *Powder Technology*, 2016; 297: 50–70.
- Zhao L, Zhou H P, Xu L Y, Song S Y, Zhang C, Yu Q X. Parameter calibration of coconut bran substrate simulation model based on discrete element and response surface methodology. *Powder Technology*, 2022; 395: 183–194.
- Ding S P, Bai L, Yao Y X, Yue B, Fu Z L, Zheng Z Q, et al. Discrete element modelling (DEM) of fertilizer dual-banding with adjustable rates. *Computers and Electronics in Agriculture*, 2018; 152: 32–39.
- Gao X J, Xie G F, Xu Y. Application of a staggered symmetrical spiral groove wheel on a quantitative feeding device and investigation of particle motion characteristics based on DEM. *Powder Technology*, 2022; 407: 117650.
- Gao X J, Zhou Z Y, Xu Y, Yu Y, Su Y, Cui T. Numerical simulation of particle motion characteristics in quantitative seed feeding system. *Powder Technology*, 2020; 367: 643–658.
- Du J, Yang Q J, Xia J F, Li G. Discrete element modeling and verification of an outer groove wheel fertilizer applicator with helical teeth. *Transactions of the ASABE*, 2020; 63(3): 659–665.
- Huang Y X, Wang B T, Yao Y X, Ding S P, Zhang J C, Zhu R X. Parameter optimization of fluted-roller meter using discrete element method. *Int J Agric & Biol Eng*, 2018; 11(6): 65–72.
- Liu W, Hu J P, Zhao X S, Pan H R, Ali Lakhari I, Wang W. Development and experimental analysis of an intelligent sensor for monitoring seed flow rate based on a seed flow reconstruction technique. *Computers and Electronics in Agriculture*, 2019; 164: 104899.
- Song C C, Zhou Z Y, Zang Y, Zhao L, Yang W, Luo X W, et al. Variable-rate control system for UAV-based granular fertilizer spreader. *Computers and Electronics in Agriculture*, 2020; 180(1): 105832.
- Song C C, Zhou Z Y, Wang G B, Wang X W, Zang Y. Optimization of the groove wheel structural parameters of UAV-based fertilizer apparatus. *Transactions of the CSAE*, 2021; 37(22): 1–10.
- Su N, Xu T S, Song L T, Wang R J, Wei Y Y. Variable rate fertilization system with adjustable active feed-roll length. *Int J Agric & Biol Eng*, 2015; 8(4): 19–26.
- Wang J F, Fu Z D, Jiang R, Song Y L, Yang D Z, Wang Z T. Influences of grooved wheel structural parameters on fertilizer discharge performance: Optimization by simulation and experiment. *Powder Technology*, 2023; 418: 118309.
- Sugirbay A M, Zhao J, Nukeshev S O, Chen J. Determination of pin-roller parameters and evaluation of the uniformity of granular fertilizer application metering devices in precision farming. *Computers and Electronics in Agriculture*, 2020; 179: 105835.
- Sun J X, Chen H M, Duan J L, Liu Z, Zhu Q C. Mechanical properties of the grooved-wheel drilling particles under multivariate interaction influenced based on 3D printing and EDEM simulation. *Computers and Electronics in Agriculture*, 2020; 172: 105329.
- Józef H, Marek M. Parameters and contact models for DEM simulations of agricultural granular materials: A review. *Biosystems Engineering*, 2016; 147: 206–225.
- Marcinkiewicz J, Selech J, Staszak Ż, Gierz Ł, Ulbrich D, Romek D. DEM simulation research of selected sowing unit elements used in a mechanical seeding drill. XXIII Polish-Slovak Scientific Conference on Machine Modelling and Simulations (MMS 2018), 2019; 254: 12. DOI: 10.1051/mateconf/201925402021.
- Liu C L, Wei D, Song L N, Li Y N, Du X, Zhang F Y. Systematic study on boundary parameters of discrete element simulation of granular fertilizer. *Transactions of the CSAM*, 2018; 49(9): 82–89. (in Chinese)
- Wang J P, Xu L, Mei S, Hu H R, Zhou J L, Chen Q. Fast and accurate detection of kiwifruits in the natural environment using improved YOLOv4. *Int J Agric & Biol Eng*, 2024; 17(5): 222–230.
- Wu Z J, Li M L, Lei X L, Wu Z Y, Jiang C K, Zhou L, et al. Simulation and parameter optimisation of a centrifugal rice seeding spreader for a UAV. *Biosystems Engineering*, 2020; 192: 275–293.